J. Fluid Mech. (1991), *vol.* 222, *pp.* 95–118
Printed in Great Britain

Turbulence in the liquid phase of a uniform bubbly air–water flow

By M. LANCE AND J. BATAILLE
Laboratoire de Mécanique des Fluides et d'Acoustique, URA CNRS 263, Ecole Centrale de Lyon, 69131 Ecully Cedex, France

(Received 6 November 1986 and in revised form 29 May 1990)

The paper describes studies of the turbulence of the liquid in a bubbly, grid-generated turbulent flow field. Laser-Doppler and hot-film anemometry are used for the experimental investigation. It is found that the turbulent kinetic energy increases strongly with the void fraction α. Roughly speaking, there exist two distinct regimes: the first one corresponds to low value of α, where hydrodynamic interactions between bubbles are negligible, and the second one to higher values, for which, owing to their mutual interactions, the bubbles transfer a greater amount of kinetic energy to the liquid. The Reynolds stress tensor shows that the quasi-isotropy is not altered. At low enough values of α, the difference between the turbulent kinetic energy in the liquid phase and the energy associated with the grid-generated turbulence proves to be approximately equal to the intensity of the pseudo-turbulence, defined as the fluctuating energy that would be induced by the motion of the bubbles under non-turbulent conditions. The one-dimensional spectra exhibit a large range of high frequencies associated with the wakes of the bubbles and the classical $-\frac{5}{3}$ power law is progressively replaced by a $-\frac{8}{3}$ dependence.

1. Introduction

Most calculations performed in gas–liquid flows for engineering purposes concern mainly headlosses in pipe flows and only require an estimation of the stress at the wall, since they are based on an integral momentum balance. Under such conditions, the friction coefficient at the wall is indeed the only really significant parameter, accounting for all forms of momentum exchange. However, in order to acquire a clear physical understanding of the mechanisms involved in any local transfer process taking place in the bulk of a turbulent dispersed two-phase flow, it is essential to determine both the magnitude and the behaviour of the Reynolds stress tensor and of the associated turbulent kinetic energy inside the continuous phase. Knowledge of such terms and their modelling is also essential if a numerical treatment of the local time-averaged equations of two-phase flows (Ishii 1975) is attempted, as for instance in the analysis of void migration (Drew & Lahey 1977, 1982) which may trigger a regime transition and affect the flow pattern. While there exists a huge number of papers dealing with wall stresses in pipes, there are comparatively few papers devoted to the determination of turbulent quantities in bubbly flows, at least when the mean diameter of the bubbles is of the order of magnitude of some turbulent lengthscale associated with the flow field of the liquid (Serizawa, Kataoka & Mishigoshi 1975; Sullivan *et al.* 1978; Theofanous & Sullivan 1982; Sato & Sekoguchi 1975; Ohba, Kishimoto & Ogasawara 1977; Lance 1979, 1986; Lance & Bataille 1983; Lance *et al.* 1980; Gherson & Lykoudis 1984; Wang 1985). Among these, the

pioneering work of Serizawa *et al.* and the recent contributions of Sullivan *et al.*, Theofanous *et al.* and Wang deserve special attention because they are quite close in spirit to the present paper. The latter give valuable information concerning void ratio profiles and turbulent intensities in a pipe flow. Unfortunately, there is a need for more data to provide a complete description of the turbulent field in the liquid, besides the fact that such a geometry makes it difficult to interpret the experimental results, in view of the highly heterogeneous character of both the basic turbulent field and the void fraction profiles. Therefore, it appeared necessary to consider the problem in a much simpler situation, that of a uniform mean flow. Specifically, the scope of the present paper is restricted to the analysis of a uniform vertical co-current air–water bubbly flow, described in §3, whose velocity and void fraction do not exceed respectively 1.2 m/s and 3%, both the diameter of the bubbles and Taylor lengthscale being of the order of 5 mm.

However unrealistic such flows might seem from a practical point of view, their study is believed to be a first step towards the investigation of somewhat more complex situations, such as shear flows (Lance, Marié & Bataille 1985). With a view to determining the above-mentioned turbulent quantities of practical interest and to give an interpretation of the mechanisms associated with the interaction between a uniform grid-generated turbulent flow and a statistically homogeneous swarm of bubbles, the authors have tried to provide a detailed and complete description of the turbulence in the liquid phase. First, the physical meaning of turbulence in two-phase dispersed flows is investigated, and the corresponding turbulent kinetic energy balance is discussed (§2). The experimental facility, the hot-film and laser-Doppler measuring techniques as well as the operating conditions are described in §3. The influence of the void fraction and of the mean liquid velocity on the various standard local parameters characterizing turbulence are examined in §4, namely the turbulent intensity, the Reynolds stress tensor, as well as the autocorrelation and uni-dimensional spectrum of the longitudinal velocity fluctuation. The isotropy of the single-phase turbulent field proves to be almost unaltered when the bubbles are injected, except possibly in the immediate vicinity of the grid. Special attention is paid to the variation of the longitudinal turbulent intensity as a function of the void fraction, which shows the existence of two turbulent flow regimes. The transition from one to the other seems to be associated with the appearance of significant hydrodynamic interactions between the bubbles at a critical value of the void fraction. Also, it is shown that at low enough void fractions, the measured turbulent kinetic energy may be considered as approximately the sum of the turbulent energy in the liquid in the absence of bubbles and the 'pseudo-turbulent' contribution associated with the motion of a swarm of identical oblate spheroidal bubbles rising along helicoidal paths in an ideal fluid. The behaviour of the one-dimensional spectra is strongly modified, especially in the high-frequency range, which obeys a $-\frac{8}{3}$ power law. A tentative explanation for this behaviour is proposed. Moreover, a careful inspection of the autocorrelation of the liquid velocity fluctuation suggests that a Taylor-type hypothesis can be reasonably invoked in order to obtain information on the spatial structure of the flow. Finally, the longitudinal evolution of the excess turbulent kinetic energy created by the bubbles results from an equilibrium between the viscous dissipation and the production due to their presence, which allows an estimation of the unknown interfacial term in the turbulent energy equation.

2. Turbulence and pseudo-turbulence in dispersed flows

Although the present study is devoted to bubbly flows, it is useful to discuss first the concept of turbulence in more general terms, for dispersed flows, i.e. gas or liquid flows carrying a large number of inclusions such as drops, bubbles, solid particles. A local and instantaneous description of such flows is generally impossible owing, among other things, to the tremendous number of initial and boundary conditions which have to be specified. It is therefore necessary to adopt a statistical description, the averaging operator being determined by the kind of problem to be treated: volume, area or segment average, time or ensemble average. The phase averages considered here (time or ensemble averages) have been well documented in the literature (Ishi 1975; Delhaye & Achard 1976; Bataille & Kestin 1981), and are given by

$$\overline{A_k}^X = \overline{\chi_k A_k}/\overline{\chi_k} = \overline{\chi_k A_k}/\alpha_k, \tag{1}$$

where A_k stands for any quantity pertaining to phase k, and χ_k is the characteristic function of phase k ($\chi_k = 1$ in phase $k, \chi_k = 0$ otherwise). The corresponding fluctuation is defined by

$$a_k = A_k - \overline{A_k}^X.$$

The associated momentum conservation equations read (see Ishii 1975)

$$\alpha_k \frac{\mathrm{d}_k}{\mathrm{d}t} \overline{\boldsymbol{U}_k}^X = -\frac{\alpha_k}{\rho_k} \nabla \overline{P_k}^X + \nabla \cdot (\overline{\boldsymbol{\tau}_k}^X + \overline{\boldsymbol{\tau}_{kT}}^X) + \alpha_k \boldsymbol{g} + \boldsymbol{M}_k, \tag{2}$$

where

$$\frac{\mathrm{d}_k}{\mathrm{d}t} = \frac{\partial}{\partial t} + \overline{\boldsymbol{U}_k}^X \cdot \nabla, \quad \overline{\boldsymbol{\tau}_{kT}}^X = -\alpha_k \overline{\boldsymbol{u}_k \otimes \boldsymbol{u}_k}^X,$$

$\boldsymbol{M}_k$ denotes the momentum exchange between the phases, $\overline{\boldsymbol{\tau}_{kT}}^X$ the averaged stress tensor and $\boldsymbol{g}$ the gravity vector.

This description amounts to replacing the initial strongly heterogeneous two-phase flow by a mixture of two coexisting equivalent fluids, with averaged physical properties. Unfortunately, however, the averaged momentum equations contain, as expected, unknown terms which require closure laws such as the correlation of the velocity fluctuations $\overline{\boldsymbol{u}_k \otimes \boldsymbol{u}_k}^X$ and the interfacial momentum transfer $\boldsymbol{M}_k$. Special attention will be paid here to the 'Reynolds-type' stress tensor.

The averaging process nevertheless exhibits some shortcomings: the averaging operator smoothes out the fluctuations existing in the continuous phase in the absence of inclusions as well as the perturbations induced by the discrete phase. The physical content of the fluctuating quantity a_k is therefore somewhat complex. In particular the velocity fluctuation in the continuous phase results from coupled mechanisms such as the turbulence of the liquid phase, originally generated by the grid, the random stirring of the continuous phase due to the motion of the inclusions, the vortex shedding in the wakes of the inclusions and the deformation of the interfaces (if any).

Obviously, neither the second nor the last contributions concern turbulent fluctuations in the usual sense. Nevertheless, they play a part in the magnitude of the velocity correlations (or the Reynolds stress tensor). In order to distinguish between 'true turbulence' and apparent turbulence, we shall call the random velocity field induced by the bubbles when no turbulent production occurs 'pseudo-turbulence'.

In order to interpret experimental results and to model the Reynolds stress tensor, it would be very useful to separate the different contributions to the velocity fluctuation, especially the part corresponding to the pseudo-turbulence. Some authors have proposed a decomposition of the instantaneous liquid velocity into

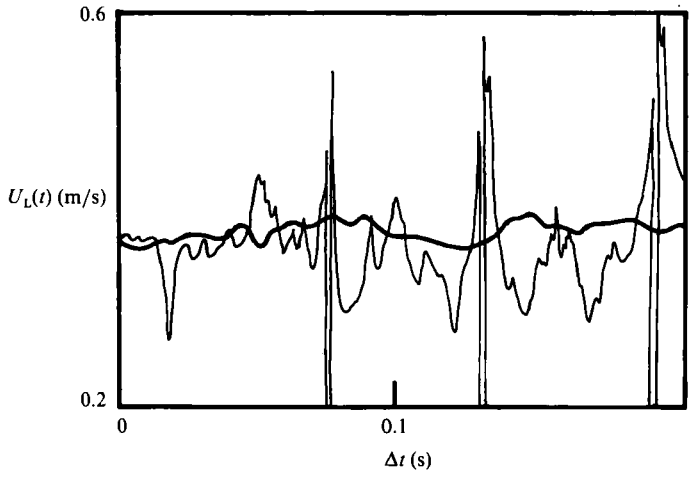

FIGURE 1. Comparison between the instantaneous liquid velocity without bubbles (heavy line) and with bubbles (thin line). Sampling frequency: 2.5 kHz.

three components: a mean value; a component due to the 'true' turbulence, and a component describing the perturbations induced by the bubbles (Sato & Sekoguchi 1975; Theofanous & Sullivan 1982). Though such a decomposition is very convenient, it has no experimental support. So far, classical filtering techniques are inoperative in view of the impossibility of defining a cut-off frequency isolating each effect. That this is indeed the case can be seen in figure 1, where a single-phase turbulent signal is compared to its two-phase equivalent.

One could introduce two different averaging operators: the first would be an ensemble average over all the configurations of the cloud of inclusions, for a given realization of the basic single-phase turbulent field; the second an ensemble average over all the realizations of the turbulent field, but for a given configuration of the cloud. Each operator allows a particular contribution to be isolated. Such a method, however, seems unrealistic, because it is impossible to control each random process separately: the motion of the inclusions is affected by the large-scale fluctuation of the turbulent field, and the turbulent eddies are distorted by the velocity gradients induced by the inclusions, at least when their mean diameter is of the order of the integral lengthscale of the single-phase turbulence.

As a consequence, in what follows a simpler approach was taken, and only a rough measure of the interaction between turbulence and pseudo-turbulence was considered, i.e. the excess turbulent kinetic energy defined as the difference between the fluctuating kinetic energy in the continuous fluid and the turbulent kinetic energy K_0 measured in the liquid in the absence of inclusions.

It proves very useful, however, to estimate *a priori* each contribution to the kinetic energy or to the Reynolds stress tensor from analytical or order-of-magnitude arguments, in the simple case of a swarm of identical bubbles of diameter D rising steadily in a quiescent liquid at a constant speed U_R.

2.1. *Contribution due to the kinematics of the bubbles: pseudo-turbulence*

According to Batchelor (1972), the ensemble average of a quantity $A(\boldsymbol{x}, t)$ attached to the liquid phase is given by

$$\langle A \rangle = \frac{1}{N!} \int A(\boldsymbol{x}, t, C_N) f(C_N) \, \mathrm{d}C_N, \tag{3}$$

where N is the number of bubbles, C_N a point in the configuration space $(x_1 \dots x_N)$, and $f(C_N)$ the probability density function for the centres. If the flow is very dispersed, the interactions between bubbles can be neglected. If, in addition, the positions of the bubbles are completely random, the above expression reduces to

$$\langle A \rangle = \frac{6\alpha}{\pi D^3} \int_{\mathscr{V}} A(\boldsymbol{x}, t)\, \mathrm{d}v, \tag{4}$$

where α is the void fraction, and $\mathscr{V}$ the volume external to the bubbles. The correlation $\overline{u_i u_j}^X$ can be easily calculated when the flow around the bubbles is given by a potential, which proves to be a reasonably good approximation in the absence of surfactants since the wakes are very thin (Moore 1963). Thus, for spherical, identical bubbles (van Wijngaarden 1982)

$$\overline{u_i u_j}^X = \langle u_i u_j \rangle = \begin{pmatrix} \frac{1}{5} & 0 & 0 \\ 0 & \frac{3}{20} & 0 \\ 0 & 0 & \frac{3}{20} \end{pmatrix} \alpha U_{\mathrm{R}}^2, \tag{5}$$

where U_{R} is the relative velocity of the bubbles with respect to the liquid.

In our experiments, the bubbles experience helicoidal trajectories. The potential for oblate spheroidal bubbles in spiralling motions is to be found in Lamb (1932) and Saffman (1956). Let Ω, d, κ, a, e denote respectively the angular velocity of the bubble, the radius of the spiral, the angle between the axis of symmetry of the bubble and the upward vertical, the longest semi-axis and the eccentricity of the bubble. The total kinetic energy T of the liquid is

$$2T = \alpha U_{\mathrm{R}}^2 \left[\left(\cos\kappa + \frac{\Omega d}{U_{\mathrm{R}}} \sin\kappa \right)^2 \frac{\gamma_0}{2-\gamma_0} + \left(\sin\kappa - \frac{\Omega d}{U_{\mathrm{R}}} \cos\kappa \right)^2 \frac{\alpha_0}{2-\alpha_0} + \frac{\Omega^2 a^2}{U_{\mathrm{R}}^2} \sin^2\kappa \frac{\alpha_0}{2-\alpha_0} \right], \tag{6}$$

where

$$\gamma_0 = 2(\zeta^2+1)(1-\zeta \arctan\zeta), \quad \alpha_0 = (\zeta^2+1)\,\zeta \arctan\zeta - \zeta^2, \quad \zeta = (1-\mathrm{e}^2)^{\frac{1}{2}}/\mathrm{e}.$$

The longitudinal kinetic energy requires numerical integrations except when the angle κ is small. In that case

$$\overline{u^2}^X = \alpha U_{\mathrm{R}}^2 f(\zeta) + \alpha \Omega^2 d^2 g(\zeta) + \alpha \Omega\, \mathrm{d} U_{\mathrm{R}}\, \kappa h(\zeta) + O(\kappa^2), \tag{7}$$

with
$$f(\zeta) = \tfrac{1}{2}(\arctan\zeta - \zeta/(1+\zeta^2))^{-2}(\arctan\zeta/\zeta + 1/(\zeta^2+1) - 2\arctan^2\zeta),$$
$$g(\zeta) = \zeta(1+\zeta^2)(2+\zeta^2-\zeta(1+\zeta^2)\arctan\zeta)^{-2}((3\zeta^2+1)\arctan\zeta - 3\zeta),$$
$$h(\zeta) = 2(f(\zeta) - g(\zeta)).$$

2.2. *Contribution due to the wakes*

The previous estimation for the kinetic energy induced by the bubbles is only valid for inviscid flows. According to Moore's (1963) work, this result is still valid for very pure liquids when the Reynolds number based on the bubble diameter is high. The wakes prove to be very thin, and can be neglected in a first approximation. Now, for tap water, the presence of surface contamination is unavoidable, and flow separation occurs on the bubble walls. For the range of bubble diameters considered in the present study (~ 5 mm), the wakes are significant and apparently turbulent (Maxworthy 1967). Therefore, the cloud of bubbles rising in the liquid can be considered equivalent to a grid, generating small-scale turbulent fluctuations, as well as the pseudo-turbulent perturbations described above. The wake contribution to

the kinetic energy can be roughly estimated from the dissipation rate, which is a fraction of the work performed by the drag force experienced by the bubbles, i.e.

$$\epsilon_w \sim \frac{\alpha}{D} C_D U_R^3, \tag{8}$$

where C_D is the drag coefficient. If one assumes that the velocity fluctuations associated with this dissipation have a lengthscale l_w, then their r.m.s. value u'_w satisfies:

$$u_w'^3/l_w \sim (\alpha/D)\, C_D U_R^3. \tag{9}$$

Thus, the energy associated with the turbulence production by the wakes is expected to vary as $\alpha^{\frac{2}{3}}$.

3. Description of the experiment

3.1. *Experimental facility*

In order to achieve the above-mentioned flow regime, a hydrodynamic tunnel (see figure 2) described in detail in Lance (1979) has been built. Its test section is a 2 m long square channel (450 × 450 mm) and it is operated at atmospheric pressure and ambient temperature, at mean liquid velocities smaller than 1.2 m/s. The grid, located upstream and made of cylindrical rods, is equipped with an array of 260 equally spaced strainless steel injectors, 0.8 mm inner diameter, through which air bubbles are blown uniformly into the tunnel (see figure 3). The void fraction thus obtained varies from 0 to 5% according to the injection pressure. The dimensions of the test section, of the grid mesh (4 cm) and the diameter of the rods (8 mm) have been selected so as to make it possible to obtain turbulent lengthscales of the same order of magnitude as the diameter of the air bubbles, to detect the smallest turbulent scales with the probes available at present, and to compare our results easily with the reference data given by Yeh & Van Atta (1973) for turbulent air flows.

In particular, the latter condition implies that the lengthscale and the Reynolds number based on the grid mesh of the turbulent water flow (in the absence of air bubbles) under consideration should be the same as those of Yeh & Van Atta's experiments for some typical mean velocity, which, here, has been chosen equal to 0.3 m/s. It is this requirement that yields the values given above for the grid mesh and the diameter of the rods. The corresponding values of the physically relevant quantities are: integral lengthscale $L_{11} = 2$ cm; Kolmogorov's lengthscale $\eta = 0.53$ mm; Reynolds number based on grid mesh $Re_M = UM/\nu = 10500$; turbulent Reynolds number $\lambda u'/\nu = 35$, where ν, λ, U, u' and M are respectively the kinematic viscosity, Taylor's lengthscale, the mean velocity, the r.m.s. value of the longitudinal velocity fluctuation u and the grid mesh.

In order to improve the isotropy of the turbulent field, a contraction section of ratio 1.27 is inserted between the grid and the beginning of the test-section (see Comte-Bellot & Corrsin 1966).

3.2. *Characterization of the basic single-phase flow*

Let X, Y and Z denote respectively the longitudinal and transversal coordinates (figure 2). The main characteristics of the flow field in the absence of bubbles, namely the mean velocity $\overline{U}$ and the turbulent intensity, were measured with the hot-film anemometer without and with the grid at various points and plotted versus Z for $X/M = 26.4$ (figure 4). The turbulent intensity is here defined as the ratio of the r.m.s.

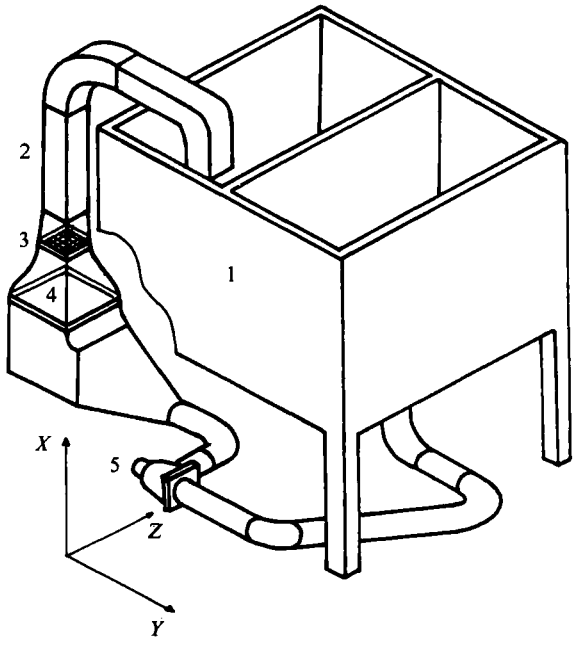

FIGURE 2. General view of the facility: 1, tank; 2, test section; 3, grid; 4, honeycomb; 5, pump.

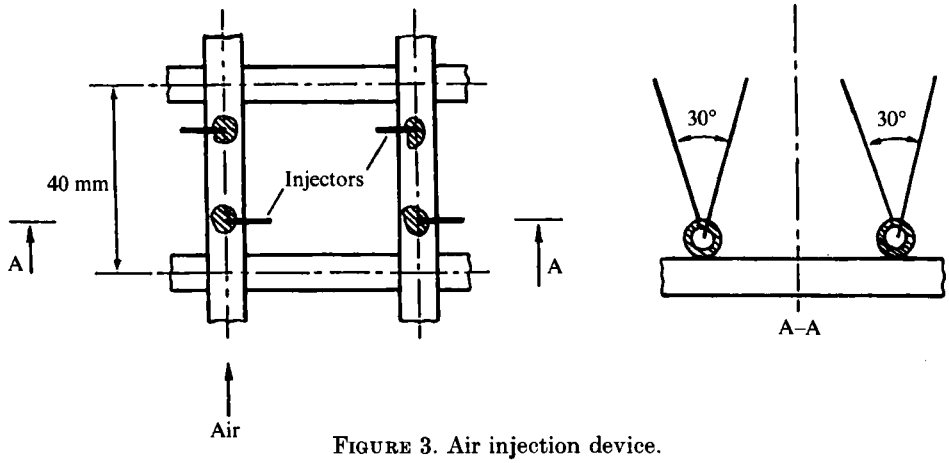

FIGURE 3. Air injection device.

value u' of the longitudinal velocity fluctuation and the mean velocity. When the tunnel is operated without the grid, the mean velocity is constant to within 0.5%, outside comparatively small boundary layers (<5 cm). In addition, the turbulent intensity, which is itself uniform in the same region, never exceeds 0.4%. Therefore, a large fraction of the volume available in the test section contains a uniform mean flow with negligible residual fluctuations.

With the grid the mean velocity and the turbulent intensity again prove to be constant along the Y-direction, to within 0.5 and 2% respectively, outside the boundary layers. The behaviour of these quantities in the Z-direction, which has been investigated using a laser-Doppler anemometer, is essentially identical. Moreover, the determination by the same technique of the ratio of the r.m.s. values

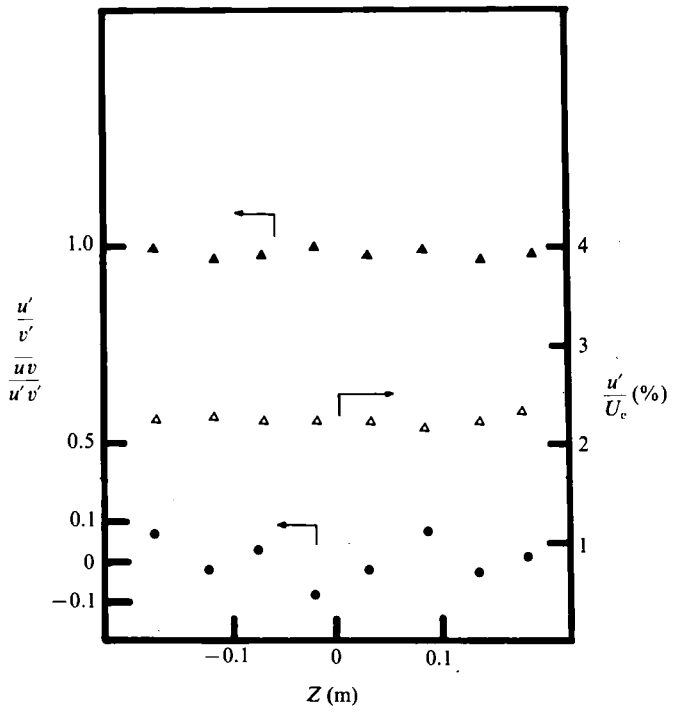

FIGURE 4. Distribution of the turbulent intensity (△), of the ratio of fluctuation u'/v' (▲), and the uv-component of the Reynolds stress tensor (●) in the Z-direction. $X/M = 26.4$, $\overline{U} = 0.45$ m/s, $\alpha = 0$.

of the longitudinal and transversal velocity fluctuations ($u'/v' = 0.98$) and of the correlation coefficient between u and v ($\overline{uv}/u'v' = 0.04$) indicate that the turbulence behind the grid is indeed isotropic (figure 4). Finally, the decay of turbulence is governed by the following asymptotic law, valid as long as $X/M > 25$ and $Re_M > 5 \times 10^3$:

$$u'/\overline{U} = \tfrac{1}{48}(X/M)^{-1.16}, \tag{10}$$

which is similar to that obtained in Comte-Bellot & Corrsin (1966) and in Yeh & Van Atta (1973).

3.3. *Instrumentation and signal processing*

An AID 7401 optical probe, detecting the change in the optical index of the medium, was employed to determine the local void ratio: the data thus obtained are known to be reliable (Galaup 1975) and were considered as reference values. The uncertainty, estimated from the experimental scattering, is of the order of 5% for an averaging time of 100 s.

The results concerning the fluctuating velocity components and other derived quantities were measured either by hot-film anemometry or by laser-Doppler anemometry.

3.3.1. *Hot-film anemometry in bubbly flow*

The measuring system was composed of a Thermosystem 1230 W conical hot-film probe, of a DISA 55 D 01 anemometer, and a DISA 55 DD 25 signal conditioner. In order to avoid the formation of bubbles at the tip of the probe, the overheat ratio of the film was restricted to 0.05. The signal was fed into a HP 1000 computer unit for numerical treatment, with a sampling frequency of 2.5 kHz selected so as to be

consistent with the highest frequencies of the signal (around 1 kHz), and with the storage capacity of the computer. It is known that the signal delivered by a hot-film probe in bubbly flow is very spiky, owing to the abrupt change of heat transfer at the crossing of the interface (Bremhorst & Gilmore 1974; Delhaye 1969). It is therefore necessary to remove the peaks from the signal before calculating the turbulence intensity. The discrimination between phases – and therefore the determination of the characteristic function χ_L of the liquid phase – was achieved by inspection of the amplitude of the quantity $(\partial u_L^2/\partial t)^2$. Such a criterion has often been adopted in single-phase turbulent intermittency experiments, for which the signal exhibits the same discontinuous behaviour (Schon & Charnay 1975; Resch 1974). The main advantage of this method is to amplify drastically the peaks on the probe due to the passage of the bubbles. A threshold value was chosen, above which the characteristic function χ_L was set equal to zero. This value was fitted so that the mean value of χ_L was equal to the local void fraction measured by the optical probe. Once the characteristic function χ_L is known, it is a straightforward matter to calculate the conditional averages of the required quantity. The mean velocity range and the integral lengthscale impose an averaging time of 200 s, in order to minimize the error due to finite time average (1 % on the turbulence intensity). However, the main source of uncertainty is due to the conditional sampling technique, for two reasons. First, the small-amplitude peaks due to incomplete piercing or to bubble sliding on the probe are difficult to detect by the present processing. Nevertheless, as the void fraction is low (<3%), these events are rare, and their contribution to the r.m.s. value of the velocity is expected to be negligible. Secondly, the void fraction measured with the conical hot film is underestimated, owing to the deformation and the deflection of bubbles by the probe, as mentioned by Wang *et al.* (1984). Therefore, the conditional sampling used here probably removes a small part of the velocity field around the bubbles, which contributes to the pseudo-turbulence. An upper bound for the relative error on the kinetic energy is $\delta\alpha U_R^2/\overline{u_L^2}^X$, where $\delta\alpha$ is the absolute error on the void fraction. A reasonable estimation for this error, based on the inspection of data scattering and comparison with laser-Doppler anemometry is 10%.

3.3.2. *Laser-Doppler anemometry*

In recent years, several attempts have been made at extending the use of laser-Doppler anemometry (LDA) to bubbly flows (Ohba *et al.* 1977; Theofanous & Sullivan 1982). In the case of very large test sections, however, a number of additional difficulties occur, mainly due to the interruption of the beams outside the measuring volume. The forward diffusion technique employed here was developed by Marié (1980, 1983) who showed that satisfactory measurements of the instantaneous velocity components could be made for void fractions of less than 7 %, provided that the signal was adequately processed by rejecting the noise due to the reflection of light on the bubbles. The optical set-up was composed of a 2.5 W Argon laser, a DISA 55 X 08 photomultiplier, a DISA 55 L 90 counter and a Bragg cell. Here, the LDA technique was essentially used to obtain the off-diagonal terms of the stress tensor by measuring the components of the velocity along two directions making $\pm 45°$ angles with the vertical axis.

3.4. *Spectral analysis*

Just like in single-phase turbulent flows, spectral analysis is expected to provide valuable information on the flow structure. Nevertheless the discontinuous character of the velocity signal delivered by hot-film anemometry makes it difficult to interpret

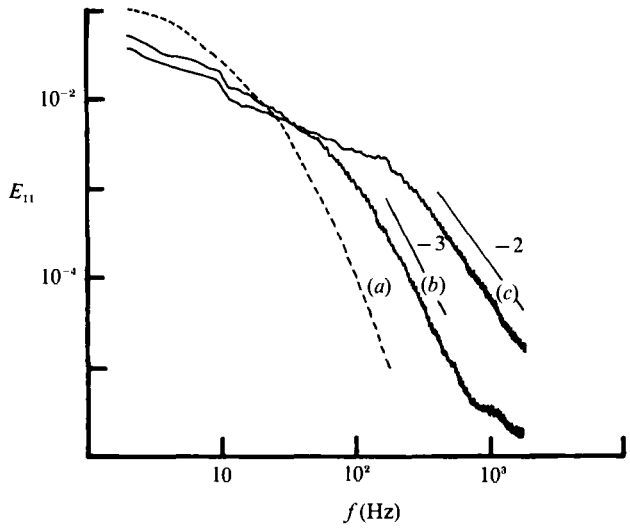

FIGURE 5. Influence of a Laplace–Gauss weighting window on the one-dimensional spectrum E_{11}. (*a*) $\alpha = 0$; (*b*) $\alpha = 1.9\%$ with window; (*c*) $\alpha = 1.9\%$ without window; $\overline{U_L}^x = 0.4$ m/s.

one-dimensional spectra. Though no definitive method has been adopted for two-phase flows, various attempts can be found in the literature: suppression of the peaks and patching together physically meaningful segments of the signal (Lance 1979; Gherson & Lykoudis 1984), linear interpolation of the velocity inside the peaks (Tsuji & Moriaka 1982), conditional sampling by the characteristic function of the liquid (Resch & Abel 1975; Lance 1979; Lee 1982). When the void fraction is small no significant difference between these techniques is observed. The last one seems preferable since it corresponds to the phase averaging defined above. However, the characteristic function χ_L is a sequence of rectangular windows which induce unphysical high frequencies for high void fraction. In order to avoid this effect, we choose to adopt a processing based on the use of weighting windows. The method consists in replacing the discontinuous function $\chi_L(x,t)$ by a sequence of smooth windows $\pi_L(x,t)$. The choice of π_L is subject to the following requirements: to minimize the deformation of the signal, which is in practice achieved when the mean value of π_L is nearly equal to $\chi_L = 1-\alpha$, and to introduce as few high frequencies as possible. This last condition is satisfied by well-known functions: Hanning, Haming, Laplace–Gauss, etc. which approximate a rectangular window while remaining of class C^∞.

In the present work, a Laplace–Gauss function was adopted. The weighted time correlation and one-dimensional spectrum of the fluctuating velocity are defined according to

$$R_{11}(t,t+\tau) = \overline{\pi_L(t)\,u_L(t)\,\pi_L(t+\tau)\,u_L(t+\tau)}/\overline{(\pi_L(t)\,u_L(t))^2} \tag{11}$$

and

$$E_{11}(\omega,t) = \frac{\overline{U_L}^x}{2\pi}\int_0^\infty R_{11}(t+\tau)\cos\omega\tau\,\mathrm{d}\tau. \tag{12}$$

The effect of the weighting window has been tested on a single frequency superposed to the characteristic function χ_L. It is checked that the peak broadening observed for the rectangular window is significantly reduced with the Laplace–Gauss windows (figure 5). The comparison between the power spectra of χ_L and π_L (figure 6) shows that the latter decreases much faster than the former, the effect on the

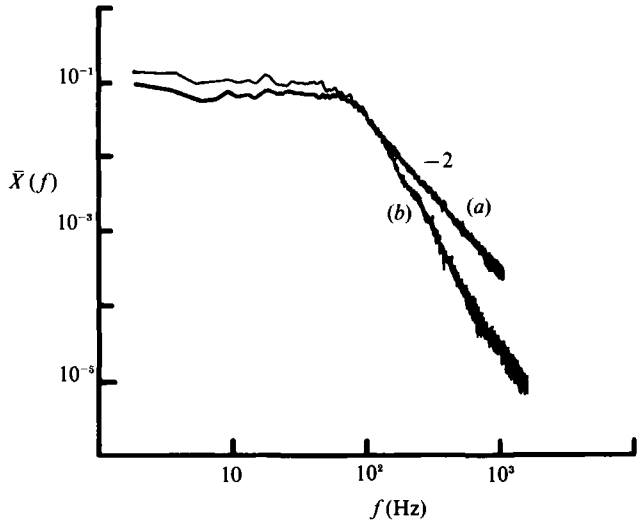

FIGURE 6. Power spectra of the characteristic function of the liquid phase: (*a*) χ_L; (*b*) π_L.

turbulence spectrum being depicted in figure 15. Owing to the low void fractions adopted in our experiments, more than 97% of the signal is representative of the liquid phase. Therefore, the distortion of the low-frequency range of the spectra is expected to be negligible.

4. Experimental results and discussion

4.1. *Controlling parameters*

It is anticipated and confirmed experimentally that sufficiently far downstream of the grid, the flow is statistically stationary and homogeneous in any horizontal plane. Therefore the behaviour of the various moments of the velocity fluctuation in the liquid phase will be governed by the following parameters: the mean velocity of the liquid $\overline{U_L}^X$, the mean velocity of the gas $\overline{U_G}^X$, the void fraction α, the mean diameter of the bubbles D, the location X of the measuring point (measured from the grid), the grid mesh M, the gravitational acceleration g, the interfacial tension σ, the mass densities ρ_L and ρ_G of the liquid and the gas, and their viscosities μ_L and μ_G. Simple physical considerations suggest that the appropriate length, time and mass scales are U_R, M and $\rho_L M^3$, where $U_R = \overline{U_G}^X - \overline{U_L}^X$ is the drift velocity. Moreover, it proves convenient to introduce an excess longitudinal turbulent kinetic energy defined by

$$u_E'^2(X) = u_L'^2(X) - u_0'^2(X), \tag{13}$$

which may be considered as a measure of the interaction between the swarm of bubbles and the original turbulent single-phase flow.

For a given grid geometry, the latter quantity may be expressed as follows in terms of non-dimensional groupings:

$$\frac{u_E'}{U_R} = F\left(\frac{X}{M}, Re_M, \alpha, Re, Fr, We, \frac{D}{M}, \frac{\rho_G}{\rho_L}, \frac{\mu_G}{\mu_L}\right), \tag{14}$$

where

$$Re_M = \frac{\rho_L \overline{U_L}^X M}{\mu_L} \tag{15}$$

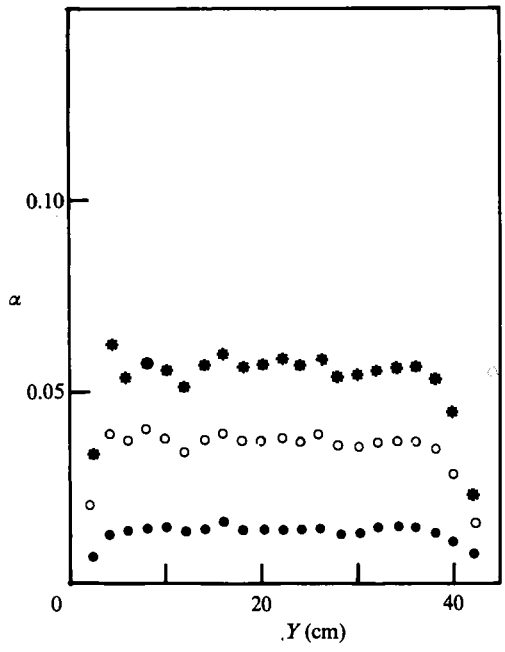

FIGURE 7. Transverse profiles of the void fraction α; $\overline{U_L}^x = 1$ m/s, $X/M = 36.4$.

is the Reynolds number based on the grid mesh, while

$$Re = \frac{\rho_L U_R D}{\mu_L}, \quad Fr = \frac{U_R^2}{gD}, \quad We = \frac{\rho_L U_R^2 D}{\sigma} \tag{16}$$

denote respectively the Reynolds, Froude and Weber numbers associated with the relative mean velocity of the bubbles.

All the experiments reported here were performed with the same grid and the same gas–liquid couple. Therefore ρ_G/ρ_L, μ_G/μ_L were constant. In view of the preceding remarks, the normalized excess turbulent kinetic energy $u_E'^2/U_R^2$ becomes a function of three independent variables only, namely: X/M, Re_M, α or of (X/M, u_0'/U_R, α), in terms of which most of the experimental results will be discussed. Their ranges of variation were respectively:

$$21.4 \leqslant X/M \leqslant 46.5; \quad 0 \leqslant u_0'/U_R \leqslant 10\%; \quad 0 \leqslant \alpha \leqslant 3\%. \tag{17}$$

Within the range of void fractions and mean liquid velocities investigated in the present work, the bubbles produced by the injection device proved to be approximately oblate spheroidal, with a mean equivalent diameter equal to 5 mm, which is of the order of magnitude of the Taylor lengthscale of the turbulence in the basic single-phase flow. The size dispersion around this value, as measured photographically, was weak and did not exceed 1 mm. The ratio of major and minor axes of the bubbles ranged from 1.8 to 2.2, and their roughly helicoidal trajectories were characterized by the spiral diameter ($1.5 < d/D < 2$), the rotation rate around the axis of the helix ($20 < \Omega < 40$ rad/s), and the angle of the spiral ($0.2 < \kappa < 0.3$ rad). The above values are consistent with the experimental observations made by Saffman (1956) and Mercier, Lyrio & Forshund (1973).

The mean rise velocity was determined from the transit time of a bubble between

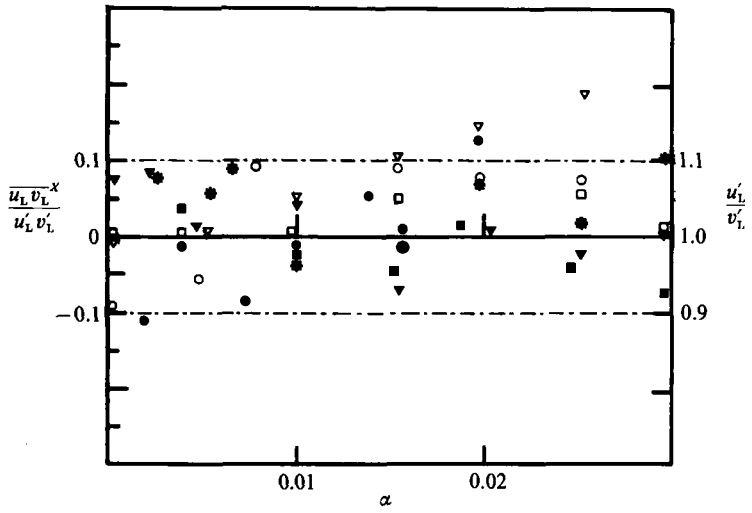

FIGURE 8. Evolution of the Reynolds-stress-tensor components as a function of the void fraction α for different values of the mean liquid velocity. Filled symbols, $\overline{u_L v_L}^X / u'_L v'_L$; open symbols, u'_L/v'_L: ○, ✱, $\overline{U_L}^X = 0.5$ m/s; ▽, ▼, $\overline{U_L}^X = 0.8$ m/s; □, ■, $\overline{U_L}^X = 0.9$ m/s; ●, $\overline{U_L}^X = 1.2$ m/s.

two film probes, 3 mm apart, and was equal to 0.24 ± 0.01 m/s. The latter value corresponds to a mean drag coefficient of 1.2.

It is worth mentioning here that, owing to the large volume of the experiment, the water was only filtered and demineralized and that surface contamination could not be completely prevented.

Finally, up till now, compressibility effects in the gas phase have been implicitly neglected. In fact, owing to the longitudinal pressure gradient associated with gravity, the mean diameter of the bubbles increases by 9% over the whole length of the test section (2 m). But, here, this variation does not exceed 3% since the two extreme stations considered were $X/M = 21.4$ and $X/M = 46.5$.

4.2. *Homogeneity and isotropy of the flow*

With the air bubbles, it is observed that except near the walls the local void fraction (figure 7), the mean velocity and turbulent intensity profiles ($u'_L/\overline{U_L}^X$) in a given section of the tunnel are flat to a good approximation – of the order of 10% – as expected for a homogeneous flow.

According to figure 8, the r.m.s. value of the transverse velocity fluctuation v'_L is practically equal to u'_L, and the off-diagonal components of the Reynolds stress tensor, such as $\overline{u_L v_L}^X$, are negligible. This property holds over the whole range of control parameters investigated. Therefore, the isotropy of the initial turbulent field is unaltered by the injection of bubbles as suggested by Theofanous & Sullivan (1982) and postulated by Drew & Lahey (1977). As a consequence only longitudinal velocity fluctuations will be considered in what follows.

4.3. *Behaviour of the longitudinal kinetic energy*

4.3.1. *Bubble-induced fluctuations in the absence of grid-generated turbulence*

In a first experiment, the air bubbles were blown through the grid for zero mean liquid velocity. The longitudinal kinetic energy was measured using the LDA technique briefly described above, for different void fractions (figure 9). Despite the

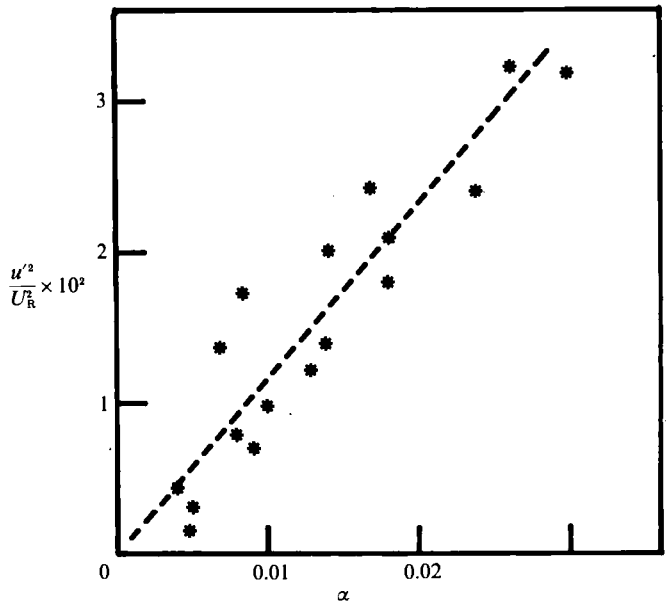

FIGURE 9. Streamwise turbulent energy for zero mean liquid velocity versus void fraction.

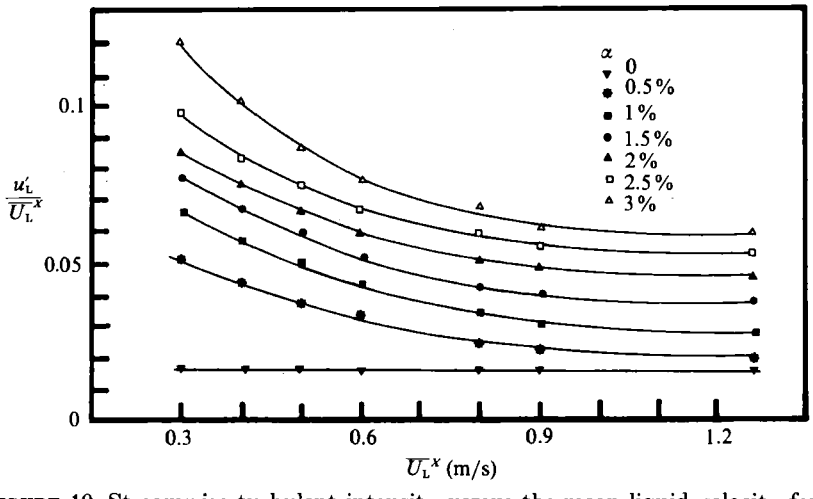

FIGURE 10. Streamwise turbulent intensity versus the mean liquid velocity for different values of the local void fraction: $X/M = 36.4$.

experimental scattering due to the existence of recirculating motion induced by the bubbles, the variation of the longitudinal kinetic energy with α exhibits a linear behaviour. Moreover, the superposition of the inviscid pseudo-turbulent contributions obtained from equation (7) and the experimental values of the parameters describing the spiralling motion of the bubbles show a reasonable agreement with the data. This result suggests that the turbulent fluctuations produced by the wakes of the bubbles contribute only a small part of the overall fluctuating kinetic energy. This statement is supported by a study of the turbulent spectra, presented in §4.4, which indicates that the high-frequency range associated with the eddies generated in the wakes represents at most 20% of the kinetic energy. Therefore, the $\alpha^{\frac{5}{3}}$ dependence expected from equation (9) is not observed here.

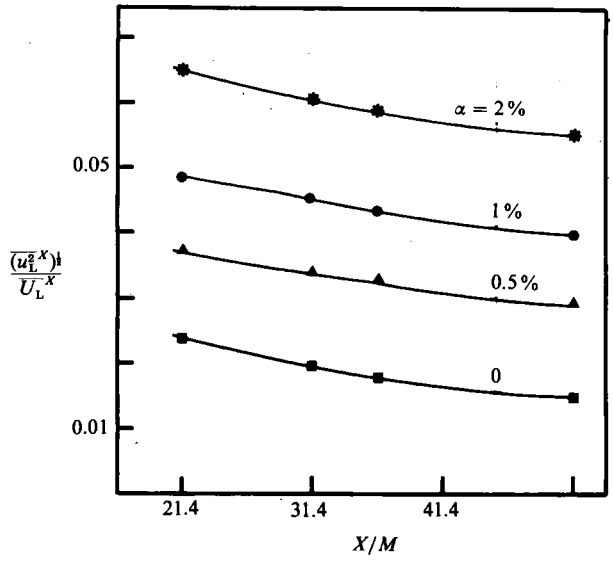

FIGURE 11. Evolution of the turbulent intensity of the liquid with the distance from the grid. $\overline{U_L}^X = 0.6$ m/s.

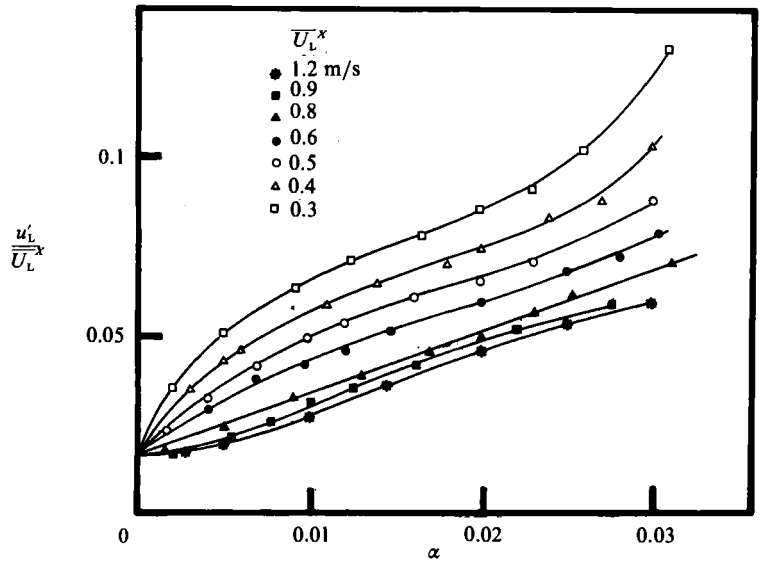

FIGURE 12. Streamwise turbulent intensity versus void fraction α: $X/M = 36.4$.

4.3.2. *Interaction between the swarm of bubbles and the grid-generated turbulence*

In order to comply with the classical presentation of single-phase turbulence, the turbulent intensity $u'_L/\overline{U_L}^X$ has first been plotted versus $\overline{U_L}^X$, X/M and α in figures 10, 11 and 12. At a given representative station X, its behaviour exhibits a strong increase with the void fraction α, depending on the value of the mean liquid velocity, while its axial variation appears to be very similar to that of the grid-generated single-phase turbulence $u'_0/\overline{U_L}$.

An equivalent but more appropriate representation in terms of the non-dimensional parameters defined in §4.1 is provided in figures 13 and 14. For any

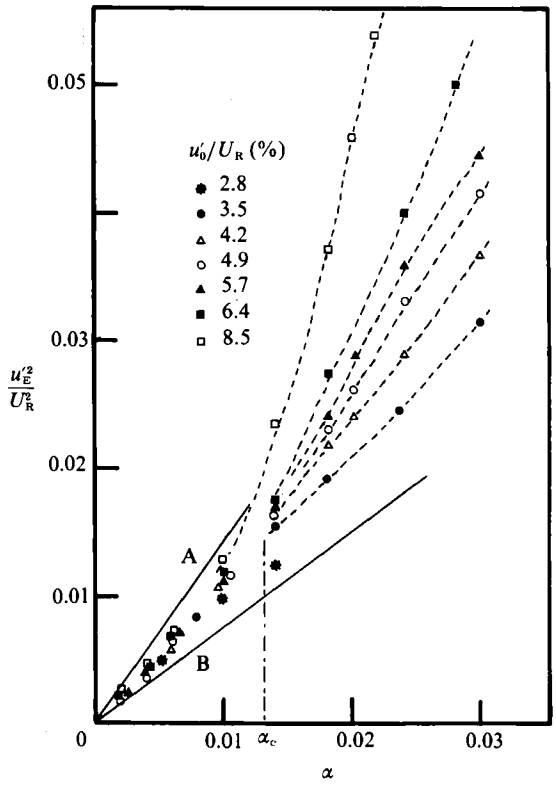

FIGURE 13. Evolution of the excess relative kinetic energy with void fraction for various values of the fluctuation generated by the grid.

given value of α and u_0'/U_R, the normalized excess turbulent intensity u_E'/U_R is seen to fluctuate, whatever X, around a constant value with an amplitude which is of the order of magnitude of experimental errors (10%), indicating that to a reasonable approximation, u_E'/U_R is a function of α and u_0'/U_R only. It is therefore convenient to consider the plane of 'operative' points whose rectangular coordinates α and u_0'/U_R account for two competitive mechanisms, the influence of the bubbles (α) and that of the basic grid-generated turbulence (u_0'/U_R). The domain of this plane, which has been experimentally investigated, reduces in fact to the region OABC shown in figure 14. The part AB of its boundary is obvious and imposed by the upper limit of the velocity of the liquid, while OCA indicates that at a given value of u_0'/U_R it proved impossible to obtain reliable data for arbitrarily high values of α, owing to the appearance of recirculation flows which destroyed the homogeneity of the motion. The non-dimensional excess turbulent kinetic energy $u_E'^2/U_R^2$ first varies linearly with α, whatever the value of the grid-generated turbulent intensity, before undergoing a slope change which depends strongly on u_0'/U_R (figure 13). This suggests the existence of two distinct regimes separated by a transitional region which can be conveniently characterized by a critical value of the void fraction α_c, defined in figure 10. Such a behaviour is best visualized in the plane of operation points $(\alpha, u_0'/U_R)$ where the critical curve $\alpha_c = \alpha_c(u_0'/U_R)$ has been drawn (figure 14). For highly dispersed flows ($\alpha < \alpha_c$), the observed linear behaviour of the excess turbulent kinetic energy is identical to that observed in the absence of the grid-generated turbulence and presented in figure 9. The good agreement (see straight lines A and B) between the

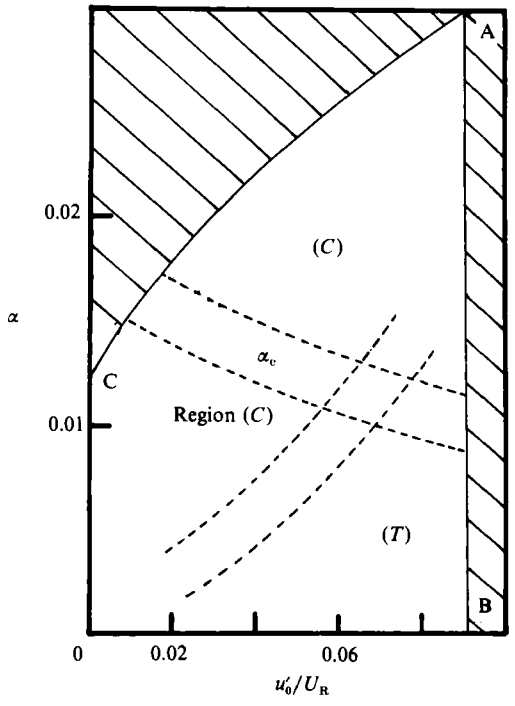

FIGURE 14. Plane of operating points $(\alpha, u_0'/U_R)$.

experimental curves and the potential flow model indicates that the kinetic energy in the liquid is a mere superposition of the turbulent energy created by the grid and that generated by the bubbles. Such a decomposition cannot of course be rigorously true since the large-scale fluctuations of the liquid velocity affect the motion of the bubbles. Nevertheless, the helicoidal model adopted here is a reasonable approximation of the actual trajectories. The contribution of the wakes to the turbulent kinetic energy remains small compared to the irrotational pseudo-turbulence for the range of bubble diameters considered here, as it was pointed out in §4.3.1. Nevertheless, the small eddies produced in the wakes of the bubbles have a strong influence on the turbulence spectra, as will be shown later.

When the void fraction increases, the mean distance between the bubbles decreases and hydrodynamic interactions begin to occur. The critical value α_c at which such interactions become significant can be estimated from the results obtained by Tsuji, Morikawa & Terashima (1982) for solid spheres at high Reynolds number. These authors have shown that interaction may appear when the transverse separation Λ between the centres of two identical solid spheres is of the order of 5 diameters. If the swarm of bubbles is considered as a random lattice of mean mesh Λ, the corresponding void fraction α_c is approximately $\alpha_c \approx (D/\Lambda)^3 \approx 10^{-2}$, which agrees with the experimental value. On the other hand, the effect of the basic grid-generated turbulence (or equivalently of the mean liquid velocity) can be explained by the following argument: owing to the large-scale velocity fluctuations in the liquid resulting from the grid turbulence, the bubbles experience large trajectory fluctuations which increase the probability of mutual hydrodynamic interactions and therefore the excess turbulent kinetic energy.

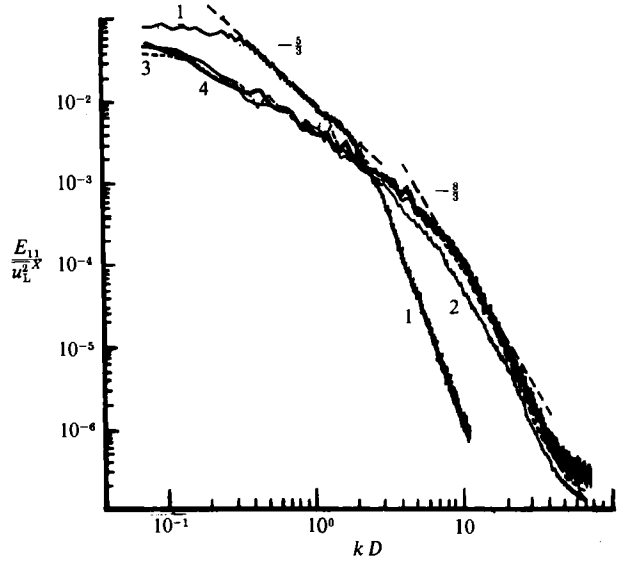

FIGURE 15. Influence of the void fraction on the one-dimensional spectrum of the velocity fluctuation in the liquid. $X/M = 36.4$. $\overline{U_L}^X = 0.9$ m/s: curve 1, $\alpha = 0$; 2, $\alpha = 1\%$; 3, $\alpha = 2.5\%$; 4, $\alpha = 4\%$.

4.4. *One-dimensional spectra and autocorrelations*

The power spectrum of the characteristic function χ_L of the liquid phase has already been shown on figure 6. The shape of the spectrum is very similar to that observed for the turbulent–non-turbulent interface in a boundary layer by Corrsin & Kistler (1953), who showed that such behaviour is typical of a Poisson statistical distribution for the appearance of discontinuities. In the present case, the Poisson law cannot be rigorously valid since the discontinuities – associated with the piercing of the bubbles by the probe – of the signal are not all independent.

Figures 15 and 16 display the one-dimensional spectra and the autocorrelations measured at the location $X/M = 36.4$, for various values of the void fraction and a given value of u'_0/U_R. Compared to the single-phase flow, it is seen that the turbulent kinetic energy of the liquid is distributed over a significantly wider range of wavenumbers. Accordingly, the associated Taylor and Kolmogorov scales are much smaller than the corresponding single-phase lengthscales (figure 17). The one-dimensional spectra and the autocorrelation curves exhibit two different behaviours, according to the domain explored in the plane of operative points (figure 14). In fact, the shape of E_{11} and R_{11} is quite independent of the void fraction in region (C), while the transition from the single phase proves to be more progressive in region (T). This suggests a competition between two mechanisms, region (C) being dominated by the pseudo-turbulence, of energy αu_R^2, and region (T) by the grid-generated turbulence, where kinetic energy is $u_0'^2$. The boundary between these domains is given by the condition $u_0'^2 \approx \alpha U_R^2$, which determines a parabolic curve in the plane $(\alpha, u'_0/U_R)$.

In region (T), the classical $-\frac{5}{3}$ power law describing the behaviour of the spectra in the high-wavenumber range is progressively replaced by another power law of exponent equal to $-\frac{8}{3}$, when the void fraction increases for a given value of u'_0/U_R. Such a feature is also seen for R_{11}, which evolves smoothly between the curves obtained for the single-phase flow and that observed in region (C).

In the latter, the autocorrelations of the velocity fluctuation show a remarkable collapse of the curves obtained for different values of α and u'_0/U_R, when plotted

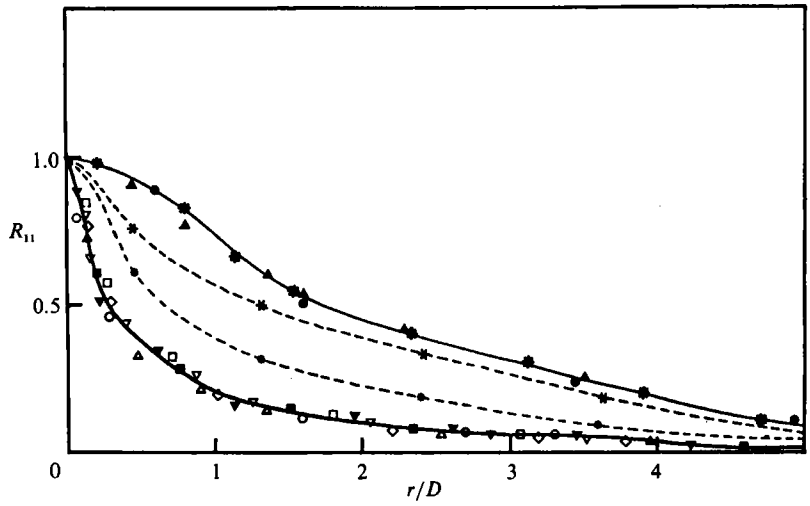

FIGURE 16. Autocorrelation of the velocity fluctuation in the liquid: ●, $\alpha = 0$, $\overline{U_L}^x = 0.3$ m/s; ✱, $\alpha = 0$, $\overline{U_L}^x = 0.78$ m/s; ○, $\alpha = 0.8\%$, $\overline{U_L}^x = 0.3$ m/s; □, $\alpha = 0.7\%$, $\overline{U_L}^x = 0.78$ m/s; ▼, $\alpha = 1.75\%$, $\overline{U_L}^x = 0.3$ m/s; ◇, $\alpha = 1.15\%$, $\overline{U_L}^x = 0.78$ m/s; ▽, $\alpha = 1.96\%$, $\overline{U_L}^x = 0.3$ m/s; ■, $\alpha = 2.32\%$, $\overline{U_L}^x = 0.78$ m/s; ▲, $\alpha = 0$, $\overline{u_L}^x = 0.91$ m/s; ✱, $\alpha = 0.7\%$, $\overline{U_L}^x = 0.91$ m/s; △, $\alpha = 2.42\%$, $\overline{U_L}^x = 0.91$ m/s; ✱, $\alpha = 1.25\%$. $\overline{U_L}^x = 0.91$ m/s.

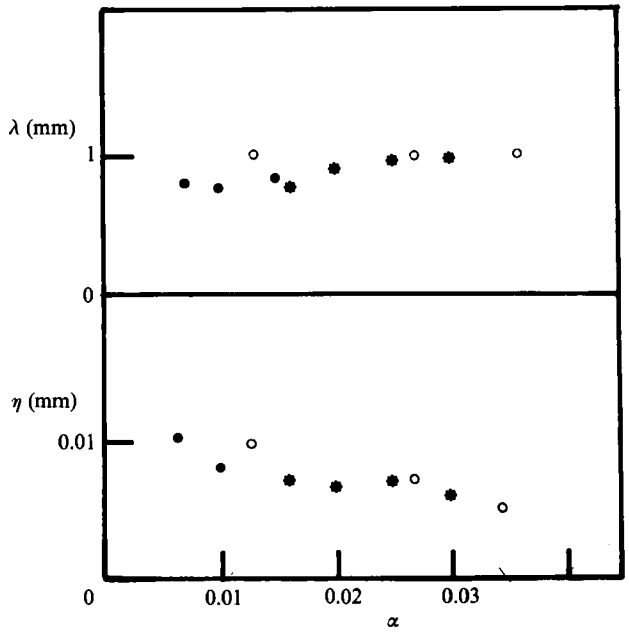

FIGURE 17. Evolution of the Taylor lengthscale λ and of the Kolmogorov lengthscale η as functions of the void fraction α. $X/M = 36.4$: ●, $\overline{U_L}^x = 0.6$ m/s; ✱, $\overline{U_L}^x = 0.7$ m/s; ○, $\overline{U_L}^x = 0.9$ m/s.

versus the non-dimensional parameter $\tau/D = \overline{U_L}^x \tau/D$. Moreover, the autocorrelation does not depend on the liquid velocity, which supports the validity of a Taylor hypothesis. The integral scale L_{11} is a constant in that domain, with $L_{11} = 0.8D$. These features bring out the existence of a well-defined structure of the flow, dominated by the motion of the bubbles.

It seems natural to associate the increase of the range of high frequencies of the spectrum with the wakes of the bubbles, which create small eddies, with a lengthscale smaller than that of the turbulent structures generated by the grid. The existence of a $-\frac{8}{3}$ power law in region (C) is however more difficult to explain. The rotational part of the turbulent field appears as a complex mixture of structures generated by the grid and of turbulent eddies produced in the bubbles' wakes. The former are created only at the inlet of the test section, while the latter are produced continuously. Owing to the viscous dissipation, the small-scale structures of the grid turbulence are very quickly dominated by that generated by the wakes. At high wavenumbers k, the spectral energy balance can be written as

$$\frac{\partial}{\partial t}E + 2\nu k^2 E = T(k,t) + \Pi(k,t), \tag{18}$$

where E is the three-dimensional turbulent spectrum, T the energy transfer, and Π the production term associated with the wakes. If the production spectrum Π is assumed to be local in the spectral space, dimensional analysis allows its functional dependence on the wavenumber to be specified. In fact, Π is a function of k and of the energy dissipation rate in the wakes, ϵ_w. This leads to the estimate $\Pi \approx k^{-1}\epsilon_w$. Now, in a stationary situation, the balance equation (18) expresses a competition between three mechanisms: viscous dissipation; spectral energy transfer; and external production, the characteristic times being respectively $\tau_D \approx \nu^{\frac{1}{2}}\epsilon_w^{-\frac{1}{2}}$, $\tau_T \approx \lambda/u'_L$, $\tau_P \approx D/U_R$. These time constants can be shown, from experimental data, to satisfy roughly the following inequalities:

$$\tau_D \leqslant \tau_P \ll \tau_T. \tag{19}$$

The eddies produced in the wakes are thus dissipated by viscosity, before spectral transfer takes place. Consequently, the spectral energy balance reduces to $2\nu k^2 E \approx k^{-1}\epsilon_w$ which leads to $E \approx k^{-3}$ in the high-wavenumber range. However crude such an estimation may appear, it is nevertheless very close to the experimental value $-\frac{8}{3}$. That the $-\frac{5}{3}$ law does not hold (except for high grid-turbulence level) is by no means surprising: indeed it seems unlikely to expect an equilibrium inertial range when the small-scale structures are continuously maintained by the bubbles. However, spectral transfer in the intermediate range is probably enhanced, the wake eddies acting as a turbulent viscosity for the large-scale structure.

At low wavenumbers, the turbulent spectrum is affected by the pseudo-turbulent fluctuations, which are dominant when u'_0/U_R is low and is therefore expected to be a function of the wavenumber and the kinetic energy transferred to the liquid by the bubbles, i.e. $E_{11} = E_{11}(k, \alpha, U_R^2)$. Dimensional analysis imposes once more $E_{11} \sim k^{-1}\alpha U_R^2$. This power law is indeed observed when α is high enough. When the energy $u_0'^2$ created by the grid becomes comparable with αU_R^2, the behaviour of the spectrum proves to be more complex, the exponent lying between $-\frac{1}{2}$ and -1.

4.5. *Decay of the kinetic energy and the interfacial production term of the fluctuating energy*

It was observed above that the excess turbulent kinetic energy does not decay along the test section. This behaviour is consistent with the splitting of the kinetic energy into two contributions, arising from the grid and from the bubbles. In fact, the pseudo-turbulence and the wakes are continuously maintained by the motions of the bubbles. On the other hand, the eddies generated by the grid experience viscous

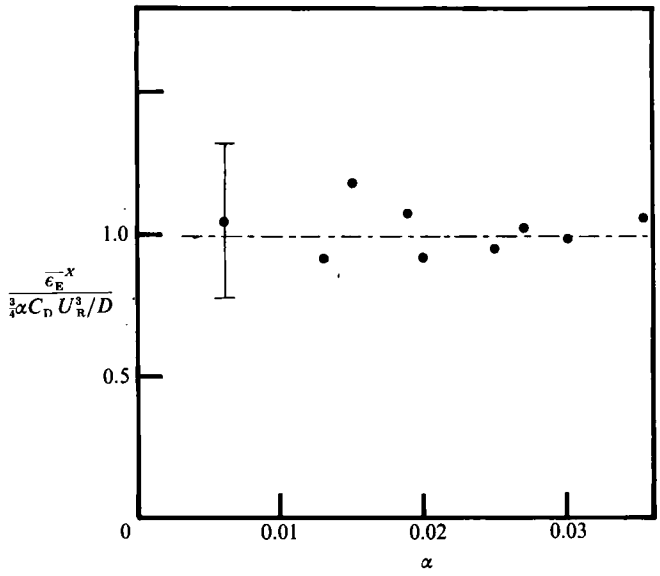

FIGURE 18. Evolution of the excess dissipation rate $\epsilon_E = \epsilon - \epsilon_0$ non-dimensionalized by the power of the drag force (measured from the spectra): $\overline{U_L}^x = 1$ m/s.

decay. From the energy balance equation, it is easily shown, using conditional averaging techniques, that the turbulence kinetic energy in the liquid K satisfies the equation

$$\frac{dK}{dt} = -\epsilon + P,$$

where ϵ is the dissipation rate in the liquid, and P an interfacial production term which need not be made explicit here. Now, the dissipation rate can be split into two parts: ϵ_0 which is associated with the eddies generated by the grid, and an excess dissipation rate, ϵ_E due to the bubbles. In view of the above result, the latter exactly counterbalances the production rate P. This property enables us to determine this interfacial production from the measurement of the dissipation rate in the liquid, which can be determined from the one-dimensional spectra of the velocity fluctuation.

The interpretation of the high-frequency range of the spectra proposed above suggests that the production P be scaled by the dissipation rate in the wakes of the bubbles, which is of the same order of magnitude as the rate of work of the drag force experienced by the bubbles, i.e. $P \sim \frac{3}{4}\alpha(C_D/D)\,U_R^3$, provided that acceleration effects due to bubble entrainment by the large eddies is small. Figure 18 shows that this estimation is consistent with the measurements.

5. Conclusions

The experimental work described here made it possible to bring out some of the striking features of the turbulence in the liquid phase of a uniform bubbly flow at low void fractions. First, the isotropy of the turbulent field is not altered by the injection of air bubbles. Moreover, within experimental errors, there exists a critical value α_c of the void fraction – of the order of 1 % – below which the turbulent kinetic energy of the liquid may be reasonably considered to be just the sum of the kinetic energy

generated by the grid and that of the 'pseudo-turbulence' associated with the motion of a cloud of non-interactive bubbles. The latter contribution is correctly estimated using a potential flow model. Above the critical value α_c, the turbulence is strongly amplified owing to the hydrodynamic interactions between the bubbles, more so as the basic grid-generated turbulence increases. Finally, when the pseudo-turbulence dominates the grid-generated turbulence, the turbulent field exhibits a specific structure, characterized by typical power laws for the one-dimensional spectra (-1 at low frequencies and $-\frac{8}{3}$ at high frequencies).

It is believed that the study of homogeneous situations can be of great help for the modelling of two-phase flow turbulence, as is the case in single-phase flow. The next step towards increasing the complexity of the study consists in the superposition a constant velocity gradient on the above configuration, in order to obtain a shear flow or a pure plane strain. Both geometries have recently been investigated and the results reported elsewhere (Lance *et al.* 1985, 1990).

The authors gratefully acknowledge the financial support of CNRS under grant ATP, and wish to thank Dr J. L. Marié for his helpful assistance in the experimental work.

REFERENCES

BATAILLE, J. & KESTIN, J. 1981 Continuum modeling of two-phase flows. *NSF rep.* GEOFLO 12.

BATCHELOR, G. K. 1972 Sedimentation in a dilute dispersion of spheres. *J. Fluid Mech.* **52**, 245–268.

BREMHORST, K. & GILMORE, D. B. 1947 Response of a hot wire anemometer probe to a stream of air bubbles in a water flow. *J. Phys.* E: *Sci. Instrum.* **9**, 347–352.

COMTE-BELLOT, G. & CORRSIN, S. 1966 The use of a contraction to improve the isotropy of a grid generated turbulence. *J. Fluid Mech.* **25**, 657–682.

COOK, T. L. & HARLOW, F. H. 1984 Virtual mass in multiphase flow. *Intl J. Multiphase Flow* **10**, 691–696.

CORRSIN, S. & KISTLER, A. L. 1953 Free-stream boundaries of turbulent flows. *NACA Rep.* 1244.

DELHAYE, J. M. 1969 Hot film anemometry in two-phase flow. *ASME Symp. on Two-Phase Flow Instrumentation, 11th Natl Heat Transfer Conf.*

DELHAYE, J. M. & ACHARD, J. L. 1976 On the averaging operators introduced in two-phase flow modeling. *OEDC Rep., Specialist's Meeting on Transient Two-Phase Flow, Toronto.*

DREW, D. E., CHENG, L. & LAHEY, R. T. 1979 The analysis of virtual mass effects in two-phase flow. *Intl J. Multiphase Flow* **5**, 233–242.

DREW, D. A. & LAHEY, R. T. 1977 Two-phase flow phenomena in nuclear reactor technology. *Q. Rep. Rensselaer Polytechnic Institute.*

DREW, D. A. & LAHEY, R. T. 1982 Phase distribution mechanisms in turbulent low-quality two-phase flow in a circular pipe. *J. Fluid Mech.* **117**, 91–106.

GALAUP, J. P. 1975 Contribution à l'étude des méthodes de mesure en écoulement diphasique. Thèse de Docteur-Ingénieur, Grenoble.

GHERSON, P. & LYKOUDIS, P. S. 1984 Local measurements in two-phase liquid-metal magneto-fluid-mechanic flow. *J. Fluid Mech.* **147**, 81–104.

HERRINGE, R. A. & DAVIS, M. R. 1976 Structural development of gas–liquid mixture flows. *J. Fluid Mech.* **73**, 97–123.

ISHII, M. 1975 *Thermo-Fluid Dynamics of Two-Phase Flows.* Paris: Eyrolles.

LAMB, H. 1932 *Hydrodynamics.* Cambridge University Press.

LANCE, M. 1979 Contribution à l'étude de la turbulence dans la phase liquide des écoulements à bulles. Thèse de Docteur-Ingénieur, Université Claude Bernard, Lyon, France.

LANCE, M. 1986 Etude de la turbulence dans les écoulements diphasiques dispersés. Thèse de Doctorat d'Etat, Lyon.

LANCE, M. & BATAILLE, J. 1983 Turbulence in the liquid phase of a bubbly air water flow. In *Proc. NATO Specialist's Meeting On Transient Two-Phase Flows, Spitzingsee.* Martinus Nijhoff.

LANCE, M., MARIÉ, J. L. & BATAILLE, J. 1985 Homogeneous turbulence in bubbly flows. In *Fundamental Aspect of Gas-Liquid Flows, Winter Annual Meeting ASME, Miami, November 1985.*

LANCE, M., MARIÉ, J. L. & BATAILLE, J. 1990 Homogeneous turbulence in bubbly flows. *Trans. ASME* I: *J. Fluids Engng* (to appear).

LANCE, M., MARIÉ, J. L., CHARNAY, G. & BATAILLE, J. 1980 Turbulence structure of a co-current air water bubbly flow. *Proc. ANS/ASME/NRC Intl Topic Meeting on Nuclear Reactor Thermal-hydraulics, 5–8 October, Saratoga Springs.*

LEE, S. J. 1982 The development of a digital data processing system for two-phase turbulence data. M.S. dissertation, Rensselaer Polytechnic Institute, Troy.

MARIÉ, J. L. 1980 Contribution au développement de l'anémométrie laser Doppler en écoulements diphasiques dispersés. Thèse de Docteur-Ingénieur, Université Claude Bernard, Lyon.

MARIÉ, J. L. 1983 Investigation of two-phase bubbly flows using LDA. *Physicochem. Hydrodyn.* **4**, 103–118.

MARIÉ, J. L., CHARNAY, G. & BATAILLE, J. 1982 Investigation of turbulence in two-phase dispersed flows using laser Doppler anemometry. *Intl Symp. on Application of LDA to Fluid Mechanics, Lisbon, June.*

MAXWORTHY, T. 1967 A note on the existence of wakes behind large rising bubbles. *J. Fluid Mech.* **27**, 367–368.

MERCIER, J., LYRIO, A. & FORSHUND, R. 1973 Three-dimensional study of the non rectilinear trajectory of air bubbly rising in water. *Trans. ASME* E: *J. Appl. Mech.* **40**, 650–654.

MOORE, D. W. 1963 The boundary layer on a spherical gas bubble. *J. Fluid Mech.* **16**, 161–176.

OHBA, A. K., KISHIMOTO, I. & OGASAWARA, M. 1977 Simultaneous measurement of local liquid velocity and void fraction in bubbly flows using a gas laser. *Tech. Rep. of the Osaka University*, vol. 27, no. 1358.

RESCH, F. 1974 Etude expérimentale de la turbulence dans les écoulements hydrauliques. Thèse de Doctorat d'Etat, Marseille.

RESCH, F. & ABEL, R. 1975 Spectral analysis using Fourier transform techniques. *Intl J. Numer. Meth. Engng* **9**, 869–902.

SAFFMAN, P. G. 1956 On the rise of small air bubbles in water. *J. Fluid Mech.* **1**, 249–275.

SATO, Y., SADATOMI, M. & SEKOGUCHI, K. 1981 Momentum and heat transfer in two-phase bubble flow. *Intl J. Multiphase Flow* **7**, 167–190.

SATO, Y. & SEKOGUCHI, K. 1975 Liquid velocity distribution in two-phase bubble flow. *Intl J. Multiphase Flow* **2**, 79.

SCHON, J. P. & CHARNAY, G. 1975 *Conditional Sampling.* Von Karman Institute, Lecture Series 73, Bruxelles.

SERIZAWA, A., KATAOKA, I. & MISHIGOSHI, I. 1975 Turbulence structure of air-water bubbly flow. *Intl J. Multiphase Flow* **2**, 221.

SULLIVAN, J. P., HOUZE, R. N., BUENGER, D. E. & THEOFANOUS, T. G. 1978 Turbulence in two-phase dispersed flows. *OECD/CSNI Specialist's Meeting on Transient Two-Phase Flows, Paris, June.*

THEOFANOUS, T. G. & SULLIVAN, J. P. 1982 Turbulence in two-phase dispersed flows. *J. Fluid Mech.* **116**, 343–362.

THOMAS, N. H., AUTON, T. R., SENE, K. & HUNT, J. C. R. 1983 Entrapment and transport of bubbles by transient large eddies in turbulent shear flows. *BHRA Intl Conf. on the Physical Modeling of Multiphase Flow, Coventry, 19–21 April.*

TSUJI, Y. & MORIAKA, Y. 1982 LDA measurements of an air–solid two-phase flow in a horizontal pipe. *J. Fluid Mech.* **120**, 385–409.

TSUJI, Y., MORIKAWA, Y. & TERASHIMA, K. 1982 Fluid-dynamic interaction between two spheres. *Intl J. Multiphase Flow* **8**, 71–82.

WANG, S. K. 1985 Three-dimensional turbulence structure measurements in air–water two-phase flow. Ph.D. thesis, Rensselaer Polytechnic Institute, Troy.

WANG, S. K., LEE, S. J., JONES, O. C. & LAHEY, R. T. 1984 Local void fraction measurement

techniques in two-phase bubbly flows using hot-film anemometry. *22th Heat Transfer Conf., Niagara Falls, 5–8 August.*

WANG, S. K., LEE, S. J., JONES, O. C., LAHEY, R. T. 1987 3-D turbulence structure and phase distribution measurements in bubbly two-phase flows. *Intl J. Multiphase Flow* **8**, 327–343.

WIJNGAARDEN, L. VAN 1976 Hydrodynamic interaction between gas bubbles in liquid. *J. Fluid Mech.* **77**, 27–44.

WIJNGAARDEN, L. VAN 1982 Hydrodynamic interactions in liquid gas flows. *Appl. Sci. Res.* **38**, 331–339.

YEH, T. T. & VAN ATTA, C. W. 1973 Spectral transfer of scalar and velocity fields in heat-grid turbulence. *J. Fluid Mech.* **58**, 233–261.